Supporting Information

Elucidation of the catalytic mechanism of a single-metal dependent homing endonuclease using QM and QM/MM approaches: The case study of I-*Ppo*I

Rajwinder Kaur, Angela Frederickson, and Stacey D. Wetmore*

Department of Chemistry and Biochemistry, University of Lethbridge, 4401 University Drive West, Lethbridge, Alberta, Canada T1K 3M4. E-mail: stacey.wetmore@uleth.ca.

Contents

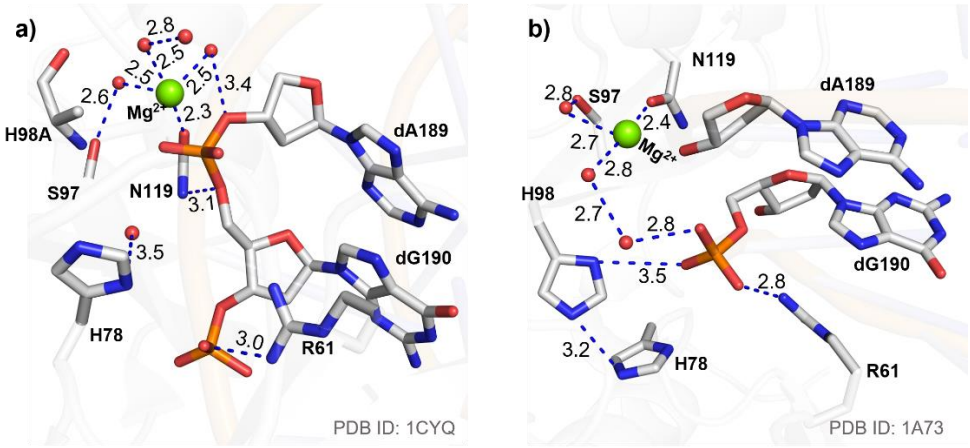

Figure S1. Key distances (Å) in the I-*Ppo*I active site based on an X-ray crystal structures of a) the Mg^{2+}-containing RC analogue of the H98A mutant or b) the Mg^{2+}-containing PC of the wild-type enzyme.

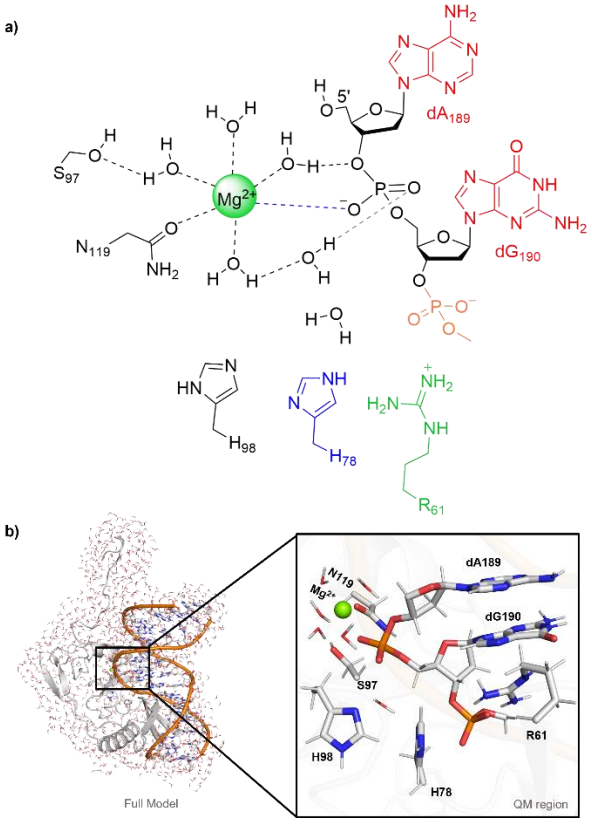

Figure S2. a) Schematic of QM cluster models involving indirect Mg^{2+} coordination to the leaving group considered in this work: Model 1 (black), Model 2 (Model 1 + H78 (blue) + expanded substrate (red)), Model 3 (Model 1 + R61 (green) + expanded substrate), Model 4 (Model 1 + H78 + R61 + 5′ phosphate moiety of dA191 on the 3′-side of dG190 (orange)). b) The corresponding enzyme–DNA QM/MM (ONIOM) model (left) and the QM region (black box, right).

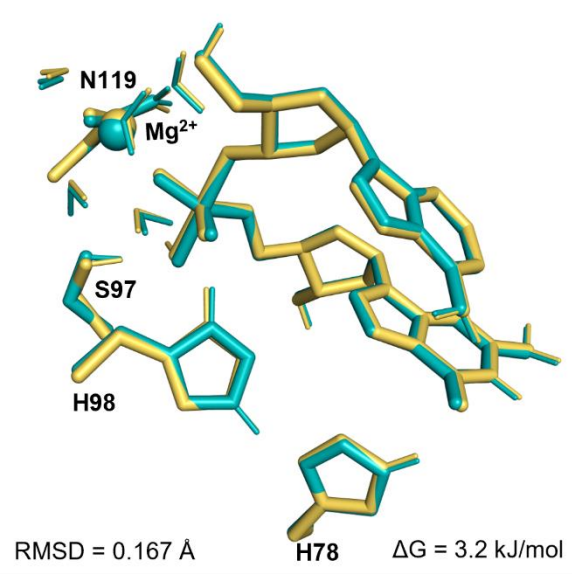

Figure S3. Overlay of the active sites of ICs obtained from the IRC corresponding to TS1 (IC, yellow) and TS2 (IC′, teal) for the phosphodiester bond cleavage pathway characterized using QM cluster Model 2 with indirect Mg^{2+} coordination to the leaving group. The energy difference was calculated for IC′ with respect to IC.

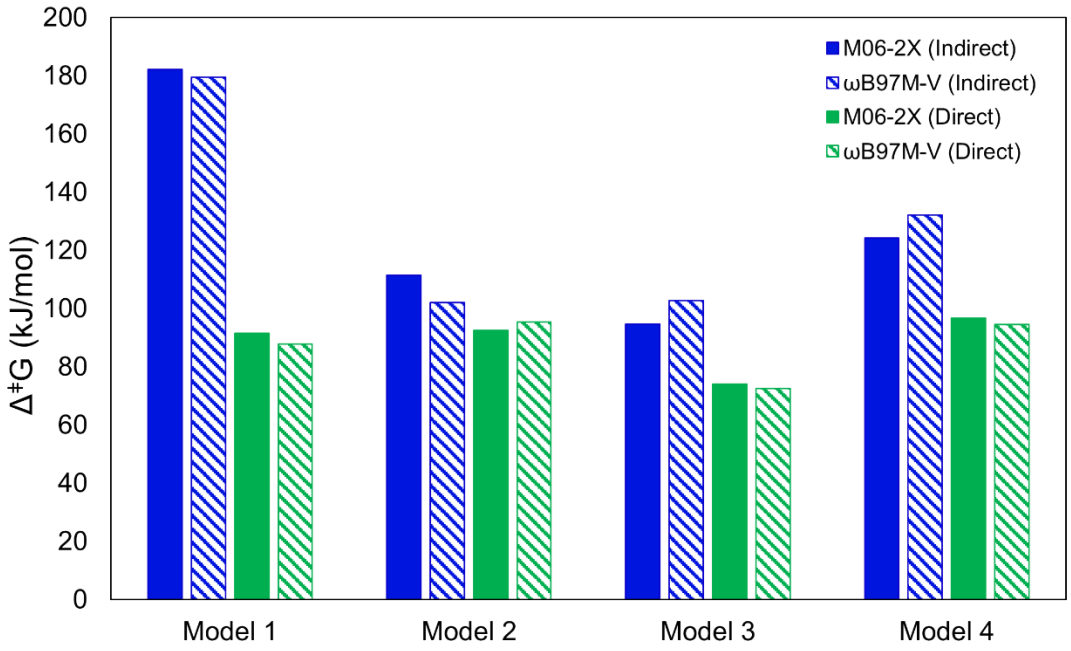

Figure S4. Comparison of the Gibbs activation energies ($\Delta^{\ddagger}G$) characterized using QM cluster models for the rate-determining step obtained using M06-2X (solid bars) and ωB97M-V (dashed bars) single-point calculations on B3LYP-D3(BJ)/6-31G(d,p) gas-phase geometries for pathways involving indirect (water-mediated, blue) or direct (green) Mg^{2+}–O3′ leaving group coordination.

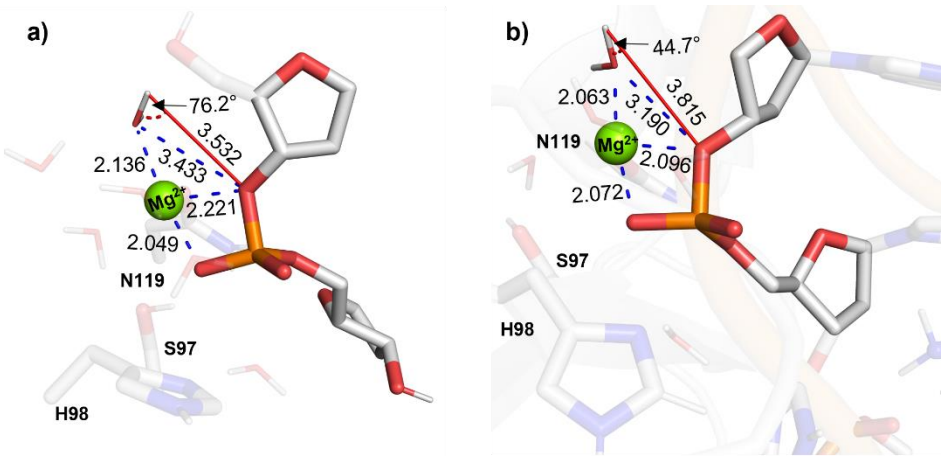

Figure S5. Key distances (Å) and angles (°) in the I-*Ppo*I active site for the RC optimized using a) QM cluster Model 1 or b) QM/MM model based on the experimentally-proposed phosphodiester bond cleavage pathway.[1]

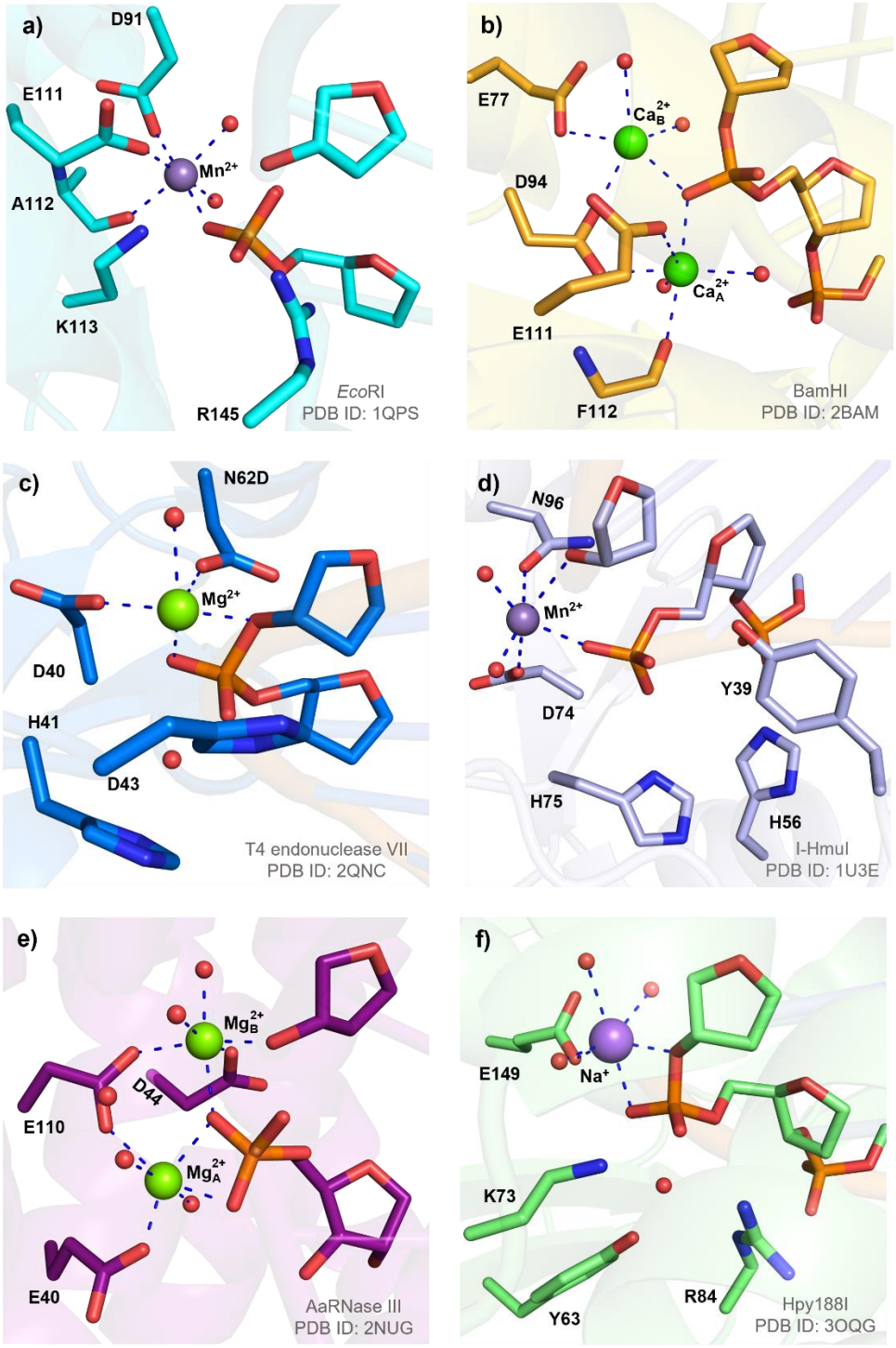

Figure S6. Active site from an X-ray crystal structure of the a) Mn^{2+}-containing PC of wild-type *Eco*RI bound to a ssDNA substrate, b) Ca^{2+}-containing RC of wild-type BamHI bound to a dsDNA substrate, c) Mg^{2+}-containing RC of the N62D mutant of T4 endonuclease VII bound to a DNA holliday junction, d) Mn^{2+}-containing PC of wild-type I-HmuI bound to a dsDNA substrate, e) Mg^{2+}-containing PC of wild-type AaRNase III bound to a dsRNA substrate, or f) Na^{+}-substituted RC of Hpy188I bound to a dsDNA substrate.

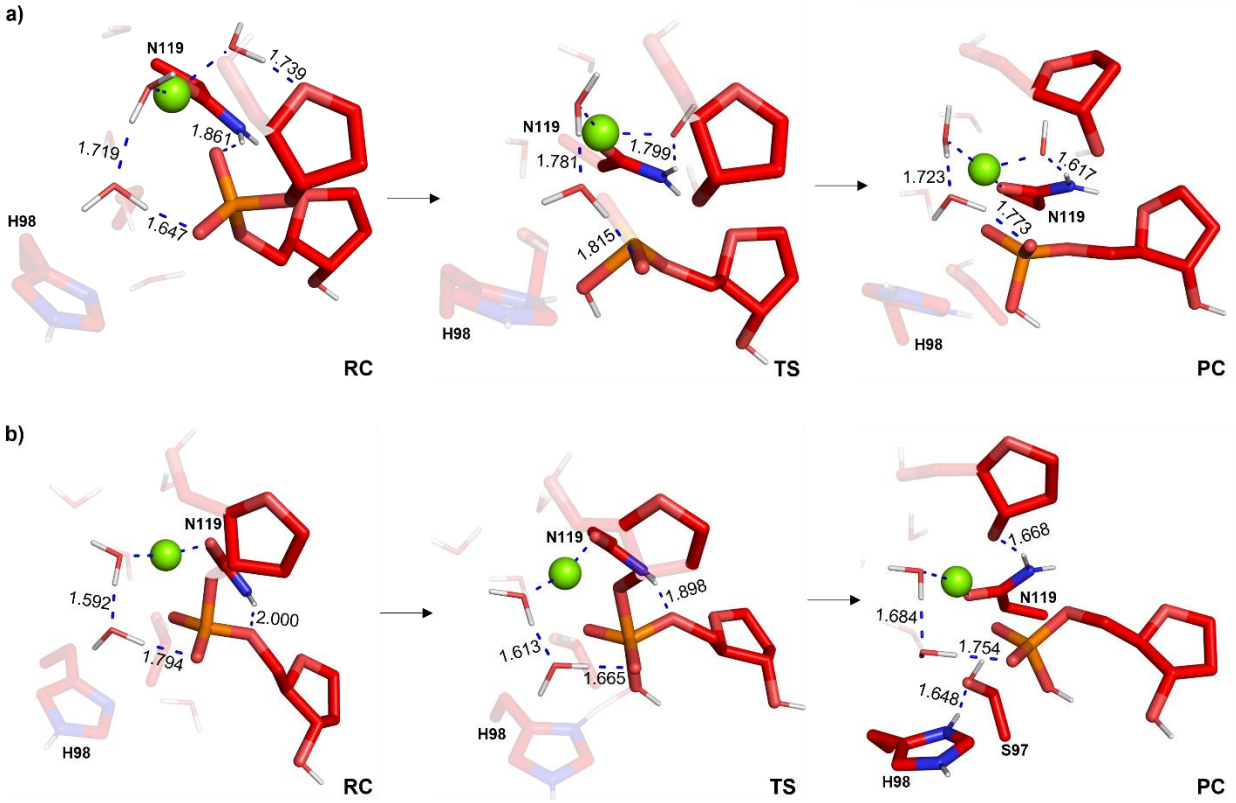

Figure S7. Key distances (Å) in the I-*Ppo*I active site for the phosphodiester bond cleavage pathway characterized using QM cluster Model 1 with a) indirect or b) direct Mg^{2+} coordination to the leaving group. See main text Figures 3b and 5b for key reaction parameters for QM cluster Model 1.

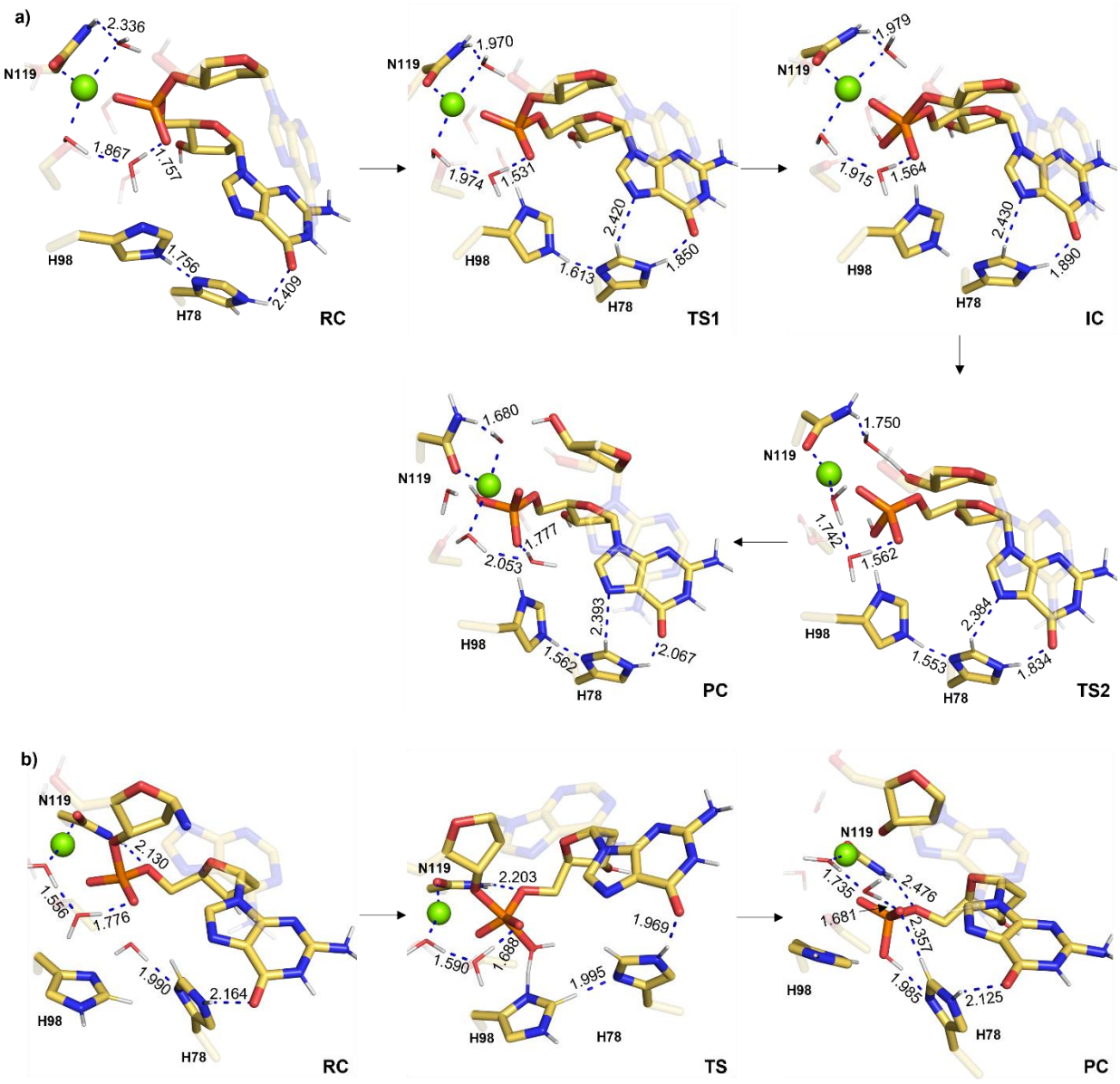

Figure S8. Key distances (Å) in the I-*Ppo*I active site for the phosphodiester bond cleavage pathway characterized using QM cluster Model 2 with a) indirect or b) direct Mg^{2+} coordination to the leaving group. See main text Figures 5b and 6 for key reaction parameters for QM cluster Model 2.

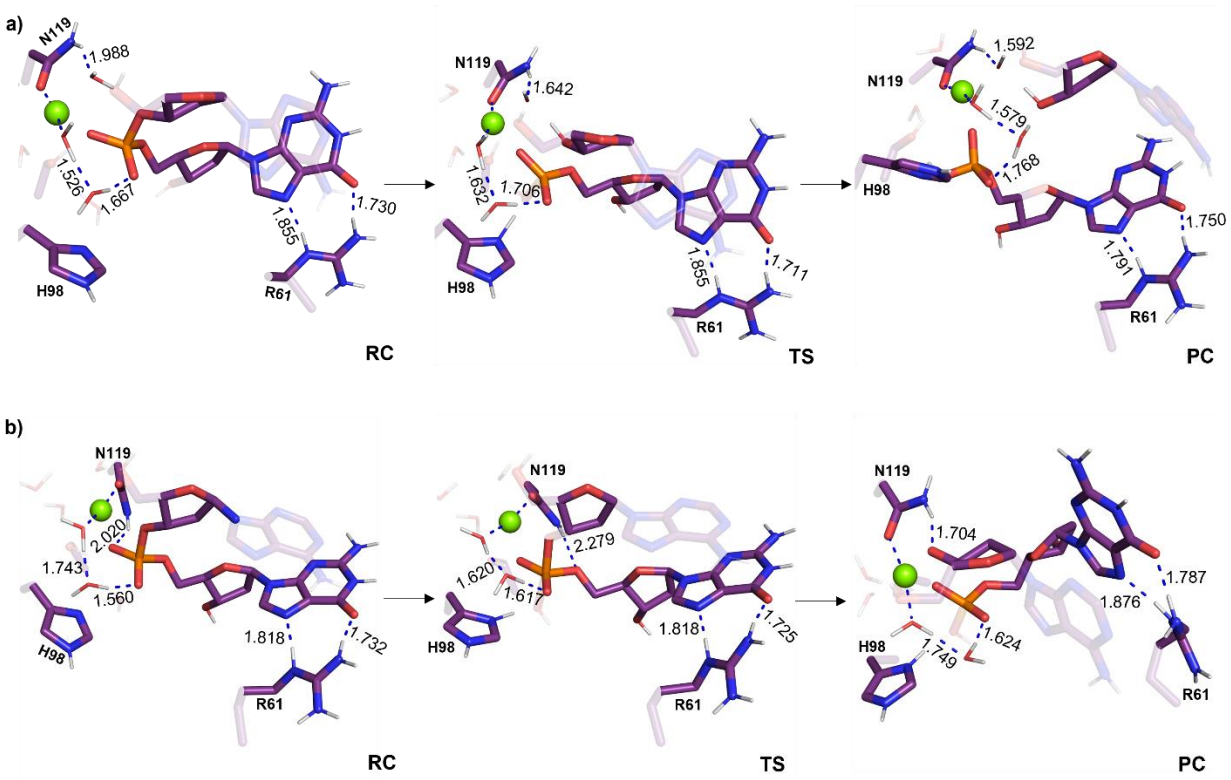

Figure S9. Key distances (Å) in the I-*Ppo*I active site for the phosphodiester bond cleavage pathway characterized using QM cluster Model 3 with a) indirect or b) direct Mg^{2+} coordination to the leaving group. See main text Figures 3b and 5b for key reaction parameters for QM cluster Model 3.

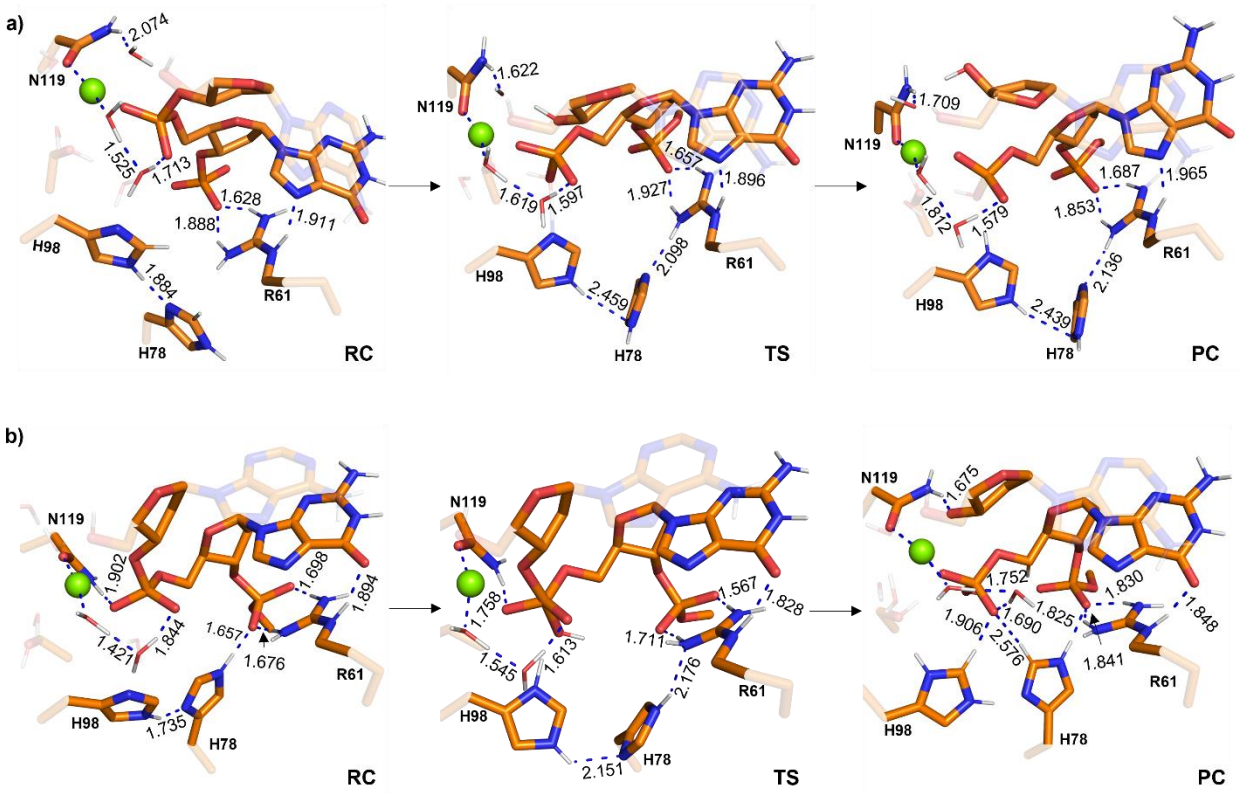

Figure S10. Key distances (Å) in the I-*Ppo*I active site for the phosphodiester bond cleavage pathway characterized using QM cluster Model 4 with a) indirect or b) direct Mg^{2+} coordination to the leaving group. See main text Figures 3b and 5b for key reaction parameters for QM cluster Model 4.

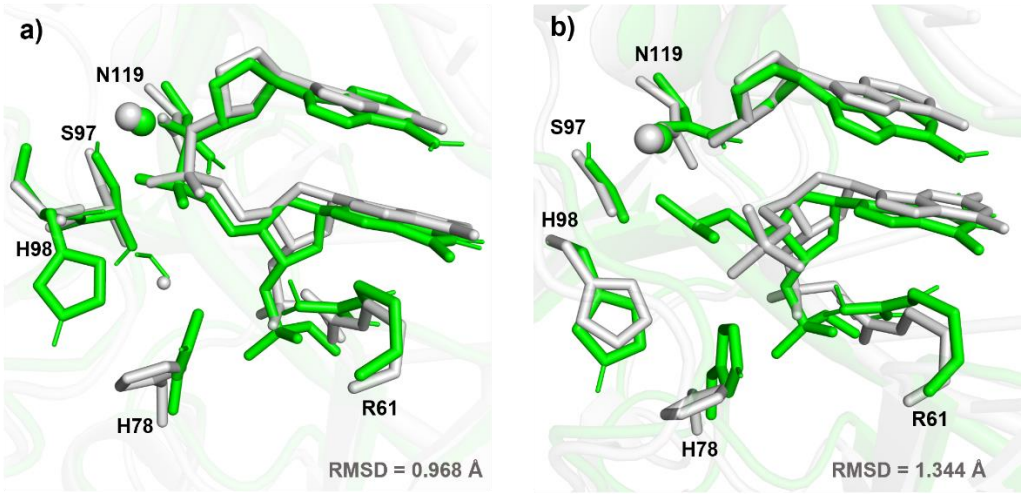

Figure S11. Overlays of the I-*Ppo*I active site comparing a) the RC from the preferred QM/MM wild-type I-*Ppo*I model (green) and the X-ray crystal structure of the H98A mutant (grey, PDB ID: 1CYQ) and b) the PC from the preferred QM/MM wild-type I-*Ppo*I model (green) and the X-ray crystal structure of wild-type I-*Ppo*I (grey, PDB ID: 1A73).

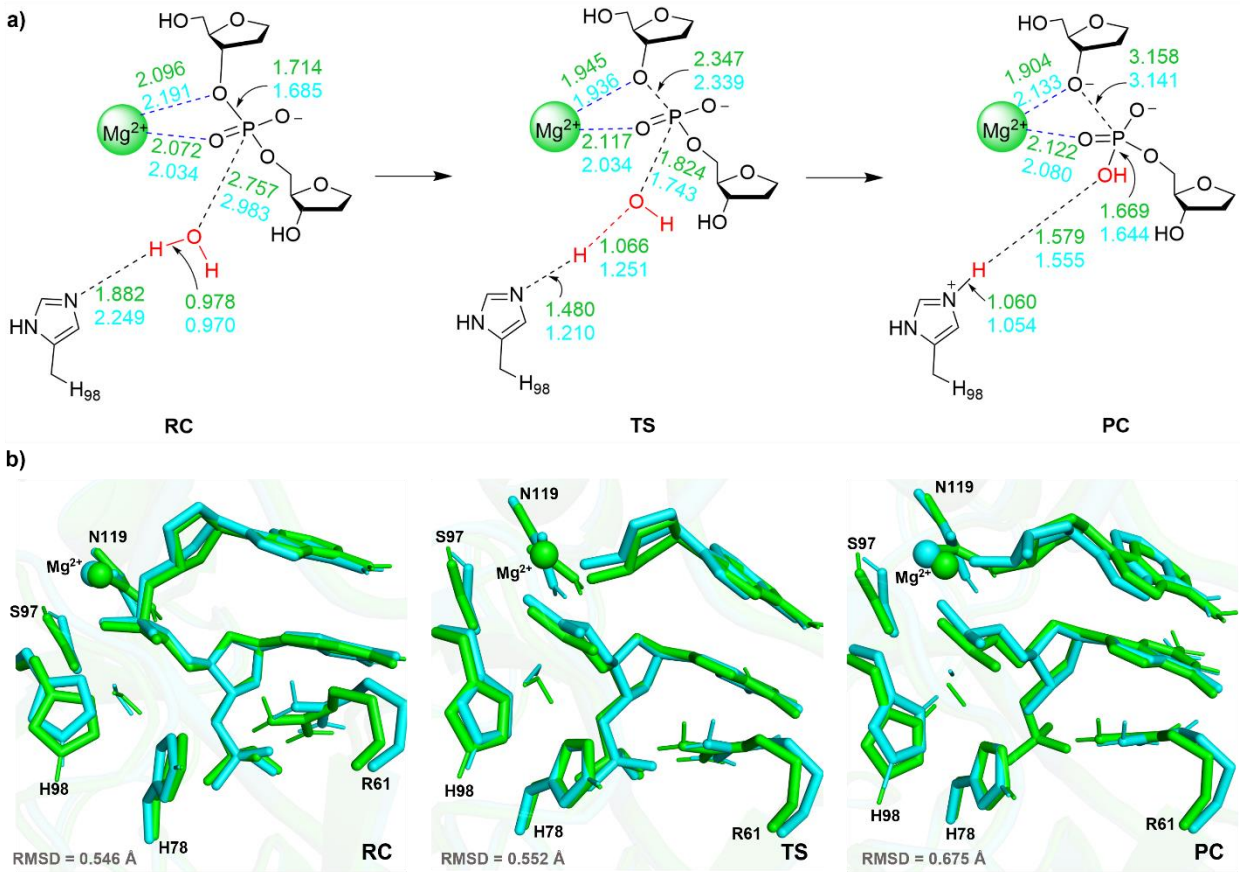

Figure S12. a) Key reaction parameters (Å) for each stationary point and b) overlays of the active site for the I-*Ppo*I catalyzed phosphodiester bond cleavage involving direct Mg^{2+} coordination to the leaving group characterized in the present work using QM/MM with mechanical (green) or electrostatic (cyan) embedding.

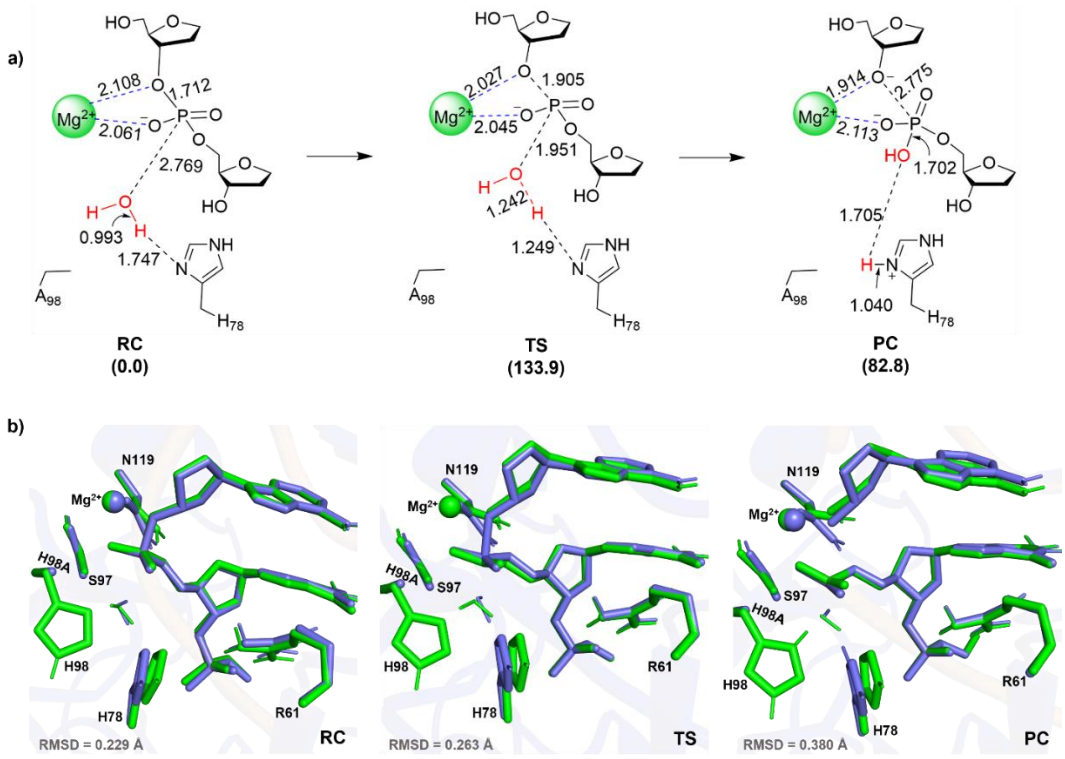

Figure S13. a) Key reaction parameters (Å) for each stationary point and relative Gibbs energies (kJ/mol, in parantheses) of the phosphodiester bond cleavage by the H98A I-*Ppo*I mutant involving direct Mg^{2+} coordination to the leaving group characterized in the present work using QM/MM and b) the corresponding overlays of the active sites of wild-type (green) and H98A I-*Ppo*I mutant (blue).

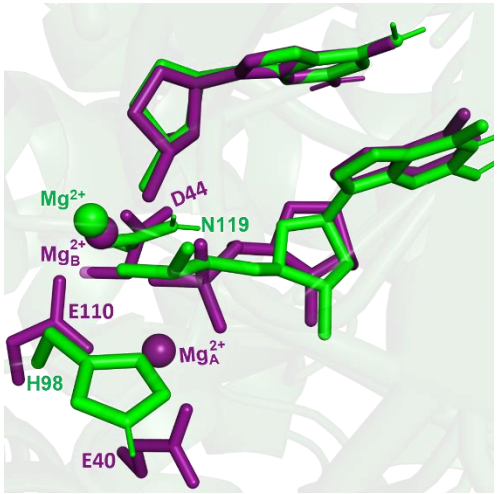

Figure S14. Overlay of the active sites of two-metal mediated AaRNase III (purple, PDB ID: 2NUG) and the preferred QM/MM PC for wild-type I-*Ppo*I (green), higlighting the similar location of Mg^{2+} with respect to the substrate.

Table S1. Relative Gibbs energies (kJ/mol) for the I-*Ppo*I facilitated phosphodiester bond cleavage characterized using QM cluster models with M06-2X or ωB97M-V (in parantheses) for the pathways involving either indirect or direct Mg^{2+} coordination to the leaving group. [a,b,c]

	RC	TS1	TS/IC	TS2	PC
Model 1 (Indirect)	0.0		182.3 (179.6)		115.0 (101.3)
Model 1 (Direct)	0.0		91.6 (87.8)		41.8 (39.4)
Model 2 (Indirect)	0.0	107.9 (102.2)	91.3 (85.2)	111.5 (103.1)	–32.8 (–35.4)
Model 2 (Direct)	0.0		92.6 (95.4)		7.4 (10.4)
Model 3 (Indirect)	0.0		94.8 (102.8)		15.4 (31.2)
Model 3 (Direct)	0.0		78.4 (72.6)		1.1 (–16.7)
Model 4 (Indirect)	0.0		124.3 (132.2)		23.2 (24.1)
Model 4 (Direct)	0.0		103.2 (94.5)		–7.8 (–17.9)

[a]Single-point calculations were carried out using Gaussian16 (rev B.01) with IEF-PCM-M06-2X/6-311+G(2df,p) (ε=4). [b]Single-point calculations were carried out using ORCA 5.0.4 with CPCM-ωB97M-V/6-311+G(2df,2p) (ε=4.9). All geometries were optimized in the gas phase using B3LYP-D3(BJ)/6-31G(d,p). [c]Refer to Figure S2 for a schematic of the QM cluster models 1 – 4.

Table S2. Relative Gibbs energies (kJ/mol) for the I-*Ppo*I facilitated phosphodiester bond cleavage characterized using QM cluster or QM/MM models for the pathway involving indirect Mg^{2+} coordination to the leaving group.[a,b,c]

	RC	TS1	TS/IC	TS2	PC
Model 1	0.0		182.3 (187.8)		115.0 (132.2)
Model 2	0.0	107.9 (108.7)	91.3 (90.9)	111.5 (113.6)	–32.8 (–33.1)
Model 3	0.0		94.8 (89.6)		15.4 (11.1)
Model 4	0.0		124.3 (128.6)		23.2 (50.1)
QM/MM	0.0		130.9		95.0

[a]Relative energies for the QM cluster models were obtained from IEF-PCM-M06-2X/6-311+G(2df,p) (ε=4) single-point calculations on B3LYP-D3(BJ)/6-31G(d,p) gas-phase geometries. Corresponding gas-phase M06-2X/6-311+G(2df,p) relative energies are provided in parentheses. [b]Relative energies for the QM/MM model were obtained from ONIOM(M06-2X/6-311+G(2df,p):AMBER) single-point calculations on ONIOM(B3LYP-D3(BJ)/6-31G(d,p) :AMBER) geometries. [c]Refer to Figure S2 for a schematic of the QM cluster models 1 – 4 and QM/MM model.

Table S3. Relative Gibbs energies (kJ/mol) for the I-*Ppo*I facilitated phosphodiester bond cleavage characterized using QM cluster or QM/MM models for the pathway involving direct Mg^{2+} coordination to the leaving group.[a,b,c]

	RC	TS	PC
Model 1	0.0	91.6 (97.6)	41.8 (54.4)
Model 2	0.0	92.6 (86.4)	7.4 (3.0)
Model 3	0.0	78.4 (80.3)	1.1 (4.5)
Model 4	0.0	103.2 (77.2)	–7.8 (21.3)
QM/MM	0.0	54.1 [77.4]	–73.8 [–101.8]

[a]Relative energies for the QM cluster models were obtained from IEF-PCM-M06-2X/6-311+G(2df,p) (ε=4) single-point calculations on B3LYP-D3(BJ)/6-31G(d,p) gas-phase geometries. Corresponding gas-phase M06-2X/6-311+G(2df,p) relative energies are provided in parentheses. QM/MM relative energies evaluated using electrostatic embedding are provided in square brackets. [b]Relative energies for the QM/MM model were obtained from ONIOM(M06-2X/6-311+G(2df,p):AMBER) single-point calculations on ONIOM(B3LYP-D3(BJ)/6-31G(d,p) :AMBER) geometries. [c]Refer to Figure 2 in the main text for a schematic of the QM cluster models 1 – 4 and QM/MM model.

Reference

1 E. A. Galburt, B. Chevalier, W. Tang, M. S. Jurica, K. E. Flick, R. J. Monnat and B. L. Stoddard, *Nat. Struct. Biol.*, 1999, **6**, 1096–1099.